Sixth-Order Resonance of High-Intensity Linear Accelerators

Dong-O Jeon,[1,*] Kyung Ryun Hwang,[2] Ji-Ho Jang,[1] Hyunchang Jin,[1] and Hyojae Jang[1]

[1]*Institute for Basic Science, Daejeon, Republic of Korea*
[2]*Department of Physics, Indiana University, Bloomington, Indiana 47405, USA*
(Received 6 February 2015; published 6 May 2015)

It is shown that the sixth-order $6\sigma = 720°$ (or $6:2$) resonance is manifested for high-intensity beams of linear accelerators through the space charge potential when the depressed phase advance per cell σ is close to and below 120° but no resonance effect is observed for σ above 120°. Simulation studies show a clear emittance growth by this resonance and a characteristic sixfold resonance structure in phase space. To verify that this is a resonance, a frequency analysis was conducted and a study was performed of crossing the resonance from above and from below the resonance. Canonical perturbation is carried out to show that this resonance arises through perturbation of strong $2\sigma = 360°$ ($2:1$) and $4\sigma = 360°$ ($4:1$) space charge resonances. Simulations also show that the space charge $6\sigma = 360°$ (or $6:1$) resonance is very weak.

Recently, many high-intensity linear accelerators (linacs) have been designed and/or constructed like the SNS (USA) [1], the J-PARC (Japan) [2], and the KOMAC (Korea) [3]. For high-intensity accelerators, it is the utmost goal to minimize the beam loss of halo particles by avoiding or minimizing contributions of various halo mechanisms. Besides mismatch [4], studies show that many nonlinear phenomena can be manifested even for a linear accelerator through the nonlinear potential of the self-field. Since the finding that the $2\nu_x - 2\nu_y = 0$ space charge (sc) coupling resonance induces halo in the ring [5], further studies of halo formation and/or emittance growth by space charge and resonances were reported in Ref. [6] and space charge coupling resonance studies of a linear accelerator such as Ref. [7]. Here, $\nu_{x(y)}$ is the horizontal (vertical) tune of a circular accelerator. A fast halo formation mechanism by a nonround beam was found for the SNS linac [8] and experimentally verified [9]. Recently, it was discovered that the $4\sigma = 360°$ (or $4:1$) resonance is manifested for high-intensity beams of linear accelerators [10] and this resonance was experimentally verified [11].

In this Letter, we report that the sixth-order $6\sigma = 720°$ ($6:2$) resonance is excited through perturbation of $2:1$ and $4:1$ resonances for high-intensity beams of linear accelerators through the space charge potential. A resonance can be expressed as $m \cdot \sigma = n \cdot 360°$, where m represents the order of the resonance and n represents the nth harmonic component of the potential. We are reporting an $m = 6$, $n = 2$ resonance that generates a sixfold resonance structure, meaning that the resonance is a sixth-order resonance driven by the second harmonic component. This resonance should not be confused with the $3\sigma = 360°$ resonance that generates a threefold resonance structure. Even-order resonances dominate because the geometry of accelerators generally has $x(y)$ midplane symmetry and generated beam distributions are symmetric and have very small skew

potential components such as $\sim x^3$ (or y^3) that drives $3\sigma = 360°$ (or $3:1$) resonance. Even though this resonance is weak compared with the fourth order $4\sigma = 360°$ space charge resonance, it is worthwhile to report this sixth-order resonance of high-intensity linear accelerators.

Numerical simulation of a linac is performed with a well-matched beam with 50 000 to 100 000 macroparticles using the PARMILA code [12]. The transverse focusing of the linac lattice is provided by an FFDD or FD [F(D): focusing (defocusing) quad] lattice. Here FFDD means an FOFODODO lattice. A 10 emA $_{40}Ar^{+10}$ beam with initial beam energy of 5 MeV/u and initial normalized rms emittance $\varepsilon_x = \varepsilon_y = 0.115 (\text{mm mrad})$, $\varepsilon_z = 0.130 (\text{mm mrad})$ is used for the simulations. The initial beam distribution is a Gaussian density distribution truncated at 3 standard deviations. The phase advance depression due to space charge effects is about $-20°$. The coupling between the transverse and longitudinal planes is minimal because the depressed longitudinal phase advance σ_z is about 10°, which is well separated from the transverse depressed phase advance.

The numerical simulations show that the $6\sigma = 720°$ resonance of high-intensity linear accelerators is manifested through the space charge potential for a variety of beams that have a nonlinear space charge potential such as Gaussian, water bag, etc. In Fig. 1, the sum of output transverse emittances is plotted vs the depressed phase advance σ of the linac lattice. Each data point is obtained by maintaining σ constant throughout a linac. No resonance effect is observed when σ is above 120° and the observed emittance growth is small, which is due to the tiny initial mismatch of the generated initial Gaussian beam.

It should be noted that maximum emittance growth takes place at around $\sigma = 112°$. For the $\sigma = 114°$ case in Fig. 1, the resonance islands are rather well separated from the main body of the beam, as shown in Fig. 2, leading to
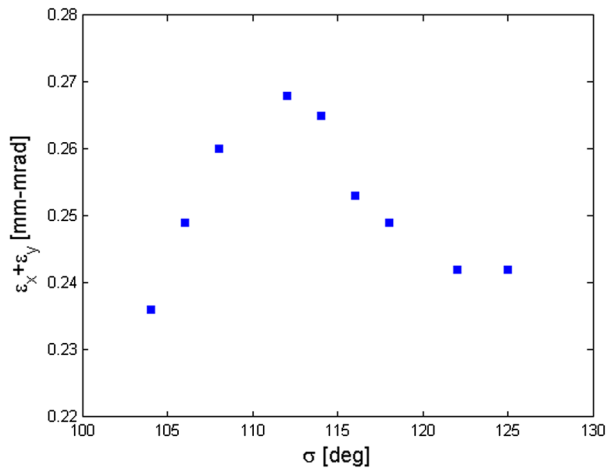
FIG. 1 (color online).   Plot of the transverse rms emittance vs depressed phase advance per cell σ showing the emittance growth induced by the $6\sigma = 720°$ (or $6{:}2$) space charge resonance of linac beams. The small emittance growth ($\sim 5\%$) observed for $>120°$ is caused by a tiny initial mismatch of the generated initial Gaussian beam.

emittance growth and a clear sixfold structure of the $6\sigma = 720°$ resonance.

One characteristic of the resonance is the behavior difference when we cross the resonance from below and from above the resonance. This is due to the stable fixed points of the resonance. When we cross the resonance from above, the six stable fixed points emerge from the origin and move away, thus scooping particles from the core (see the plots of Fig. 3, as we cross the resonance from above). On the other hand, when we cross the resonance from below, stable fixed points move in from afar toward the
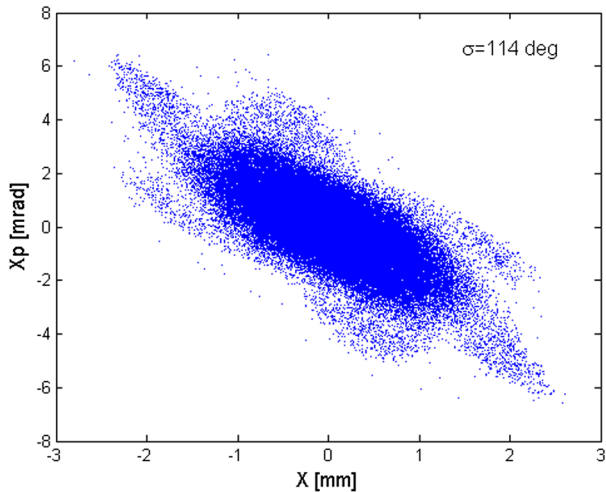

FIG. 2 (color online).   Plot of the beam distribution in phase space for the linac case with $\sigma = 114°$ in Fig. 1. Six stable islands are rather well separated from the main body of the beam. The depressed phase advance σ is maintained fairly constant throughout the linac lattice.
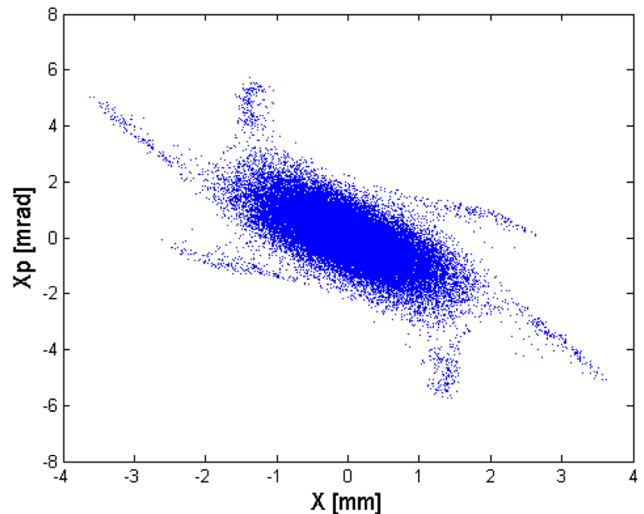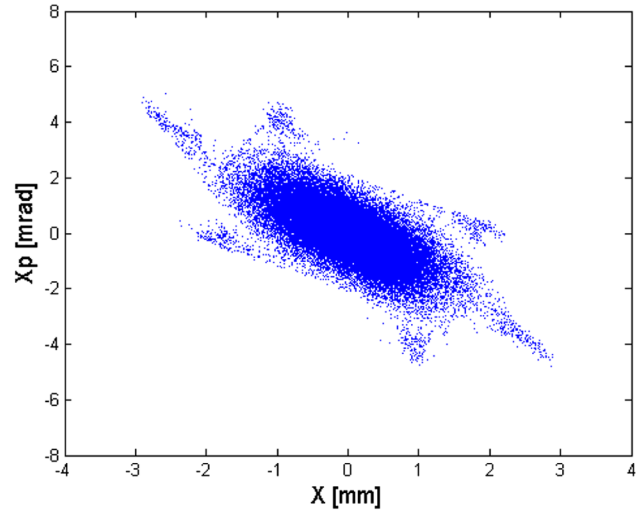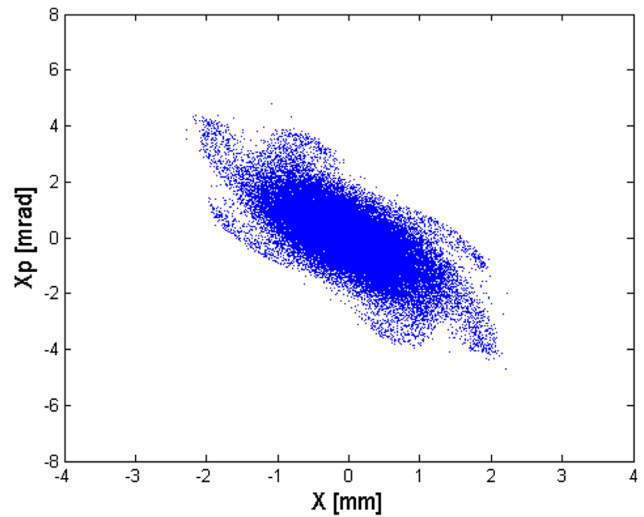

FIG. 3 (color online).   Plots of beam distribution evolution as one crosses the $6\sigma = 720°$ (or $6{:}2$) resonance from above the resonance (from the top to the bottom plot in sequential order). One observes that the six stable fixed points emerge from the origin and move away, scooping particles.
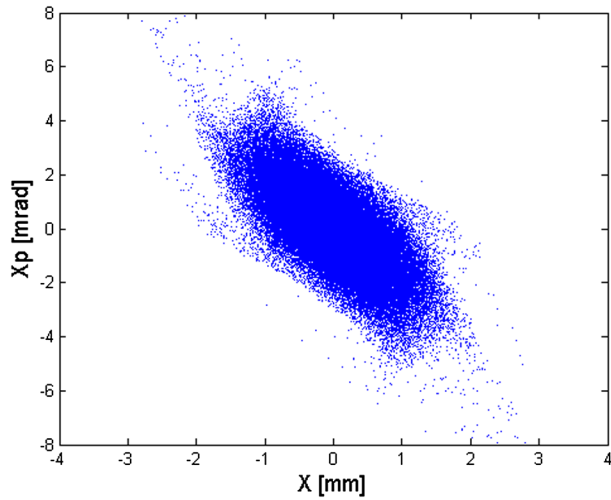
FIG. 4 (color online).   Plot of beam distribution as one crosses the $6\sigma = 720°$ (or 6:2) resonance from below the resonance. One observes that the particles are not captured by the stable fixed points and they move around stable islands.
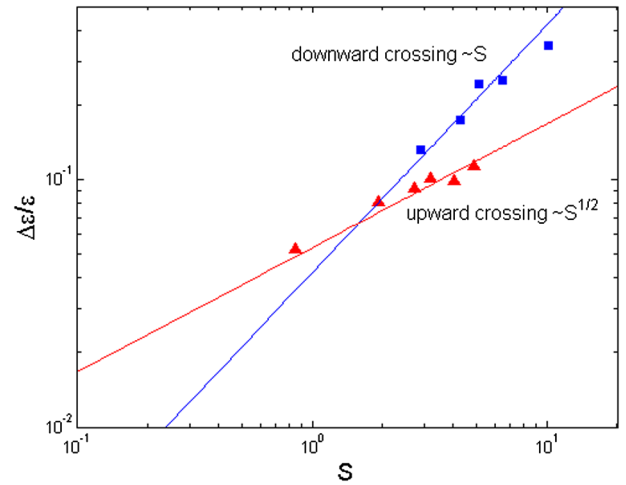

FIG. 5 (color online).   Plot of emittance growth when one crosses the $6\sigma = 720°$ resonance from above (downward crossing) and from below (upward crossing). Here S is defined as $S = (\Delta\sigma/360°)^2/(d\sigma/dn/360°)$, where $\Delta\sigma$ is the tune depression (proportional to the stopband width of the resonance) and $d\sigma/dn$ is the phase advance change per cell.

origin. So the particles cannot be captured by the stable fixed points, and they move around the fixed points (see Fig. 4). Figure 3 illustrates how the beam distribution evolves as one crosses the resonance from above the resonance, where σ varies from 121° to 108° (downward crossing) along the linac lattice. The plots from top to bottom show how six stable fixed points move away from the beam. On the other hand, when one crosses the resonance from below the resonance (upward crossing), stable fixed points move in from afar toward the origin and the particles cannot be captured by the stable fixed points. Particles, rather, move around the fixed points as shown in Fig. 4.

Depending on the direction to cross the $6\sigma = 720°$ resonance, the emittance growth also differs for the same reason. Figure 5 shows the plot of emittance growth of resonance crossing vs a parameter $S = (\Delta\sigma/360°)^2/(d\sigma/dn/360°)$ [13,14], where $\Delta\sigma[=2\pi[\xi_x + (G_2^2/\delta_2)]$ [in Eq. (10)] is the tune spread (proportional to the stopband width of the resonance [14]) and $d\sigma/dn$ is the phase advance change per cell. The parameter S is equivalent to $g^2/(\Delta\nu/\Delta n)$ in Ref. [13] and is a measure of how fast the resonance crossing is and how strong the resonance is. Two groups of data show a distinct difference due to the resonance characteristics. It should be noted that the emittance growth for the upward crossing scales as $S^{1/2}$, while emittance growth scales as S for the downward crossing. A large value of S means slow resonance crossing or wide resonance stopband.

Another characteristic of the resonance is the existence of a resonant frequency component. Due to the fixed points of the resonance, some particles have the same frequency as the driving frequency of the $6\sigma = 720°$ resonance. A Fourier analysis is performed on the rms beam size

along the linac lattices with $\sigma = 112°$ and $125°$, respectively. A clear $6\sigma = 720°$ resonance peak is observed at the particle tune value of $1/3$ ($=120°/360°$) for the linac with $\sigma = 112°$, as shown in Fig. 6. Here, particle tune is defined

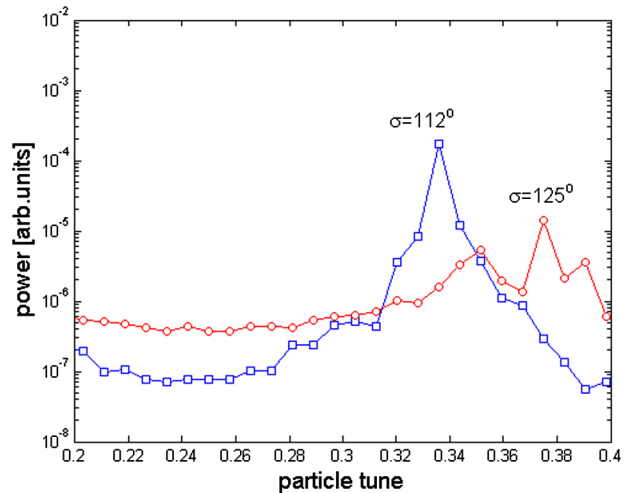FIG. 6 (color online).   Plot of power spectrum of the frequency analysis on the rms beam size (second-order moment) for $\sigma = 112°$ and $125°$. The particle tune is defined as the number of transverse oscillations that individual particles make over one period. When particles are trapped by the sixth-order resonance stable islands, they make $1/3$ turn over one lattice cell. For the case with $\sigma < 120°$, we see a clear $6\sigma = 720°$ resonance peak at the tune of $1/3$ ($120°/360°$), while no resonance peak is observed for the case with $\sigma > 120°$. It is observed that the space charge $6\sigma = 360°$ resonance is very weak and we observe practically no emittance growth associated with this resonance for a wide range of σ.

as the number of transverse oscillations particles make over one cell. No resonance peak is observed at the tune of $1/3$ when $\sigma = 125°$ just above the resonance. It is evident that there is no resonance effect when $\sigma > 120°$.

Simulations also show that the space charge $6\sigma = 360°$ resonance is very weak and no emittance growth is

observed. This demonstrates that the $6\sigma = 720°$ resonance is not from the x^6 term of the space charge potential in Eq. (2). To understand the $6\sigma = 2 \cdot 360°$ (or $6:2$) resonance, we explore the space charge Hamiltonian for a 2D Gaussian beam, given by

$$H(\boldsymbol{x},\boldsymbol{p};s) = \frac{p_x^2 + p_y^2}{2} + \frac{K_x}{2}x^2 + \frac{K_y}{2}y^2 + V_{sc}, \tag{1}$$

$$V_{sc} = -\frac{K_{sc}}{2}\left[\frac{x^2}{a(a+b)} + \frac{y^2}{b(b+a)}\right] + \frac{K_{sc}}{8a^2(a+b)^2}\left[\frac{2+r}{3}x^4 + \frac{2}{r}x^2y^2 + \frac{1+2r}{3r^3}y^4\right]$$
$$-\frac{K_{sc}}{144a^3(a+b)^3}\left[\frac{8+9r+3r^2}{5}x^6 + \frac{3(3+r)}{r}x^4y^2 + \frac{3(3r+1)}{r^3}x^2y^4 + \frac{8r^2+9r+3}{5r^5}y^6\right] + \cdots, \tag{2}$$

where s is the longitudinal coordinate on reference orbit, $K_x(s)$ and $K_y(s)$ are focusing field strength, $a^2 = \beta_x\varepsilon_x$ and $b^2 = \beta_y\varepsilon_y$ are beam size, and $r = b/a$. Since we are interested in the $6:2$ resonance in horizontal plane, the 1D Hamiltonian can be approximated as

$$H = \frac{p_x^2}{2} + K_x\frac{x^2}{2} - V_2x^2 + V_4x^4 - V_6x^6 + \cdots, \tag{3}$$

where V_i are coefficients with space charge potential.

Since K_x, V_2, and V_4 are periodic functions of period L, using Floquet transformation with, $x = \sqrt{2\beta_xJ_x}\cos\Phi_x$, where $\Phi_x = \varphi_x + \chi_x - \nu_x\theta$ with $\chi_x = \int_0^s(1/\beta_x)ds$, $\nu_x = \sigma/360°$, $\theta = 2\pi s/L$, and J_x and Φ_x are canonical conjugate variables, we obtain the Hamiltonian as follows:

$$H = \nu_xJ_x - \frac{L}{2\pi}V_2\beta_xJ_x - \frac{L}{2\pi}V_2\beta_xJ_x\cos 2\Phi_x$$
$$+ \frac{L}{2\pi}V_4\beta_x^2J_x^2\frac{3 + 4\cos 2\Phi_x + \cos 4\Phi_x}{2}. \tag{4}$$

To study resonance, we carry out Fourier decomposition to the Hamiltonian in lattice harmonics. Since both $2:1$ and $4:1$ resonances are relevant to $6:2$ resonance, we approximate the Hamiltonian as follows:

$$H = \nu_xJ_x - \xi_xJ_x + \alpha_{xx}\frac{J_x^2}{2} + G_2J_x\cos(2\varphi_x - \theta + \eta_2)$$
$$+ G_4J_x^2\cos(4\varphi_x - \theta + \eta_4) + \cdots, \tag{5}$$

where

$$\xi_x = \frac{1}{2\pi}\int_0^L V_2\beta_xds, \qquad \alpha_{xx} = \frac{3}{2\pi}\int_0^L V_4\beta_x^2ds,$$

$$G_2e^{i\eta_2} = -\frac{1}{2\pi}\int_0^L V_2\beta_xe^{i[2\chi_x - (2\nu_x - 1)\theta]}ds,$$

and

$$G_4e^{i\eta_4} = \frac{1}{4\pi}\int_0^L V_4\beta_x^2e^{i[4\chi_x - (4\nu_x - 1)\theta]}ds.$$

The $6:2$ resonance of the space charge potential in Eq. (3) is weak as apparently shown in numerical simulations. In order to understand the strong $6:2$ resonance, we need to carry out canonical perturbation to strong $2:1$ and $4:1$ resonances.

It is known that a resonance can be produced by two strong resonances, e.g., $2:1$ and $4:1$ resonances can generate a $6:2$ resonance. Using a generating function,

$$F_2(\varphi_x, I_x) = \varphi_xI_x + B_2(I_x)\sin(2\varphi_x - \theta + \eta_2)$$
$$+ B_4(I_x)\sin(4\varphi_x - \theta + \eta_4), \tag{6}$$

where (φ_x, J_x) and (ψ_x, I_x) are old and new conjugate phase space coordinates, and B_2 and B_4 terms are chosen to cancel out the $2:1$ and $4:1$ resonances, respectively, we find the new Hamiltonian as

$$\check{H} \approx \nu_xI_x - \xi_xI_x + \alpha_{xx}\frac{I_x^2}{2} + (\nu_x - \xi_x + \alpha_{xx}I_x)\Delta J + \frac{\alpha_{xx}}{2}\Delta J^2$$
$$+ (I_xG_2 - B_2)C_2 + (I_x^2G_4 - B_4)C_4$$
$$+ (2I_xC_4G_4 - C_2G_2)\Delta J, \tag{7}$$

where $\Delta J = J_x - I_x = 2B_2C_2 + 4B_4C_4$, $S_n = \sin(n\varphi_x - \theta + \eta_x)$, and $C_n = \cos(n\varphi_x - \theta + \eta_x)$.

The new Hamiltonian becomes

$$
\begin{aligned}
\check{H} = {} & \nu_x I_x - \xi_x I_x + \alpha_{xx}\frac{I_x^2}{2} + (2B_2G_2 + 2B_2\alpha_{xx})C_2^2 \\
& + (8B_4G_4I_x + 8B_4^2\alpha_{xx})C_4^2 \\
& + (G_2I_x + \delta_2 B_2 + 2B_2\alpha_{xx}I_x)C_2 \\
& + (G_4I_x^2 + \delta_4 B_4 + 4B_4\alpha_{xx}I_x)C_4 \\
& + (4B_4G_2 + 4B_2G_4I_x + 8B_2B_4\alpha_{xx})C_2C_4,
\end{aligned}
\tag{8}
$$

where C_2 and C_4 corresponds to the $2\!:\!1$ and $4\!:\!1$ resonance driving terms, C_2C_4 can be combined into the $6\!:\!2$ resonance, and $\delta_n = n(\nu_x - \xi_x) - 1$.

Setting $B_2 = -[G_2I_x/(\delta_2 + 2\alpha_{xx}I_x)]$, $B_4 = -[G_4I_x^2/(\delta_4 + 4\alpha_{xx}I_x)]$ to remove the $2\!:\!1$ and $4\!:\!1$ resonances in the Hamiltonian, and identifying $\langle C_n^2 \rangle = \langle S_n^2 \rangle = 1/2$ for detuning, we obtain

$$
\begin{aligned}
\check{H} \approx {} & \left(\nu_x - \xi_x - \frac{G_2^2}{\delta_2}\right)I_x + \alpha_{xx}\left(1 + 6\frac{G_2^2}{\delta_2^2}\right)\frac{I_x^2}{2} \\
& + G_{6:2}I_x^2 \cos(6\psi_x - 2\theta + \eta_2 + \eta_4),
\end{aligned}
\tag{9}
$$

with $G_{6:2} = -2(G_2G_4/\delta_2\delta_4)(6\nu_x - 6\xi_x - 2)$ near the $6\!:\!2$ resonance. The resonance driving term is explicitly shown above. When the betatron tune is near $2/6$, we find $\delta_2 < 0$, $\delta_4 > 0$ and $(6\nu_x - 6\xi_x - 2) > 0$; thus $G_{6:2} > 0$. We also note that the resonance driving strength is proportional to I_x^2 instead of I_x^3 of the normal $6\!:\!1$ or $6\!:\!2$ resonances.

The Hamiltonian near the $6\!:\!2$ resonance is given by Eq. (9). We transform the Hamiltonian into resonance rotating frame by the canonical transformation $F_2 = (\psi_x - \frac{1}{3}\theta + \frac{1}{6}\eta_2 + \frac{1}{6}\eta_4)I$, we find the conjugate phase space coordinates $I = I_x$, and $\psi = (\psi_x - \frac{1}{3}\theta + \frac{1}{6}\eta_2 + \frac{1}{6}\eta_4)$. The new Hamiltonian is

$$
\begin{aligned}
H = {} & \left(\nu_x - \frac{1}{3} - \xi_x - \frac{G_2^2}{\delta_2}\right)I + \alpha_{xx}\left(1 + 6\frac{G_2^2}{\delta_2^2}\right)\frac{I^2}{2} \\
& + G_{6:2}I^2 \cos 6\psi.
\end{aligned}
\tag{10}
$$

Analysis of this Hamiltonian shows clearly that the $6\!:\!2$ resonance must occur when $\nu_x - \xi_x - (G_2^2/\delta_2) < \frac{1}{3}$ (or $\sigma < 120°$) as shown in the numerical simulations.

The most important result presented in this Letter is that the sixth-order $6\sigma = 720°$ resonance in high-intensity linear accelerators arises through the second-order perturbation to strong $2\sigma = 360°$ (or $2\!:\!1$) and $4\sigma = 360°$ (or $4\!:\!1$)

space charge resonances. Canonical perturbation was performed and the final Hamiltonian is used to prove that the resonance has to occur below the 120 degree, not above.

*Corresponding author.
jeond@ibs.re.kr

[1] J. Stovall *et al.*, *Proceedings of the 2001 Particle Accelerator Conference, Chicago* (IEEE, New York, 2001), p. 446.

[2] Y. Yamazaki, *Proceedings of the 2003 Particle Accelerator Conference, Portland* (IEEE, New York, 2003), p. 576.

[3] Byung-Ho Choi, *Proceedings of the 2004 Asian Particle Accelerator Conference, Gyeongju, Korea*, (IEEE, New York, 2004), p. 231.

[4] J. D. Lawson, *The Physics of Charged Particle Beams*, 2nd ed. (Oxford University Press, New York, 1988).

[5] D. Jeon, J. A. Holmes, V. V. Danilov, J. D. Galambos, and D. K. Olsen, Phys. Rev. E **60**, 7479 (1999).

[6] X. Huang, S. Y. Lee, K. Y. Ng, and Y. Su, Phys. Rev. ST Accel. Beams **9**, 014202 (2006).

[7] G. Franchetti, I. Hofmann, and D. Jeon, Phys. Rev. Lett. **88**, 254802 (2002).

[8] D. Jeon, J. Stovall, A. Aleksandrov, J. Wei, J. Staples, R. Keller, L. Young, H. Takeda, and S. Nath, Phys. Rev. ST Accel. Beams **5**, 094201 (2002).

[9] D. Jeon, Phys. Rev. ST Accel. Beams **16**, 040103 (2013).

[10] D. Jeon, L. Groening, and G. Franchetti, Phys. Rev. ST Accel. Beams **12**, 054204 (2009).

[11] L. Groening, W. Barth, W. Bayer, G. Clemente, L. Dahl, P. Forck, P. Gerhard, I. Hofmann, M. S. Kaiser, M. Maier, S. Mickat, T. Milosic, D. Jeon, and D. Uriot, Phys. Rev. Lett. **102**, 234801 (2009).

[12] H. Takeda and J. Stovall, *Proceedings of the 1995 Particle Accelerator Conference, Dallas* (IEEE, New York, 1995), p. 2364.

[13] S. Y. Lee, Phys. Rev. Lett. **97**, 104801 (2006).

[14] S. Y. Lee, G. Franchetti, I. Hofmann, F. Wang, and L. Yang, *New J. Phys.* 8, 291 (2006); I. Hofmann and G. Franchetti, *Proceedings of the 2007 Particle Accelerator Conference, Albuquerque* (IEEE, New York, 2007), p. 3259.